Applied Catalysis B: Environmental 314 (2022) 121390

Contents lists available at ScienceDirect

Applied Catalysis B: Environmental

journal homepage: www.elsevier.com/locate/apcatb

Activating peroxymonosulfate by N and O co-doped porous carbon for efficient BPA degradation: A re-visit to the removal mechanism and the effects of surface unpaired electrons

Yong-Li He [a,b], Chuan-Shu He [a,b,*], Lei-Duo Lai [a,b], Peng Zhou [a,b], Heng Zhang [a,b], Ling-Li Li [a,b], Zhao-Kun Xiong [a,b], Yang Mu [c], Zhi-Cheng Pan [d], Gang Yao [e], Bo Lai [a,b,*]

[a] State Key Laboratory of Hydraulics and Mountain River Engineering, College of Architecture and Environment, Sichuan University, Chengdu 610065, China
[b] Sino-German Centre for Water and Health Research, Sichuan University, Chengdu 610065, China
[c] CAS Key Laboratory of Urban Pollutant Conversion, Department of Environmental Science and Engineering, University of Science and Technology of China, Hefei 230026, China
[d] Laboratory of Wastewater Treatment Technology in Sichuan Province, Haitian Water Group, Chengdu 610065, China
[e] Institute of Environmental Engineering, RWTH Aachen University, Germany

ARTICLE INFO

Keywords:
Bisphenol A degradation
PMS activation
Heteroatom doping
Unpaired electrons
Carbon catalysis

ABSTRACT

In this study, N and O co-doping carbon materials with porous structure (NOPC-x) were applied to activate peroxymonosulfate (PMS) for bisphenol (BPA) degradation and the underlying effects in affecting NOPC-x activity were revealed. Electrochemical characterization, electron paramagnetic resonance (EPR) tests, quenching and PMS adsorption experiments were applied to clarify the mechanism of BPA degradation. It's found that BPA can be completely removed within 20 min (k_{obs} = 0.30 min^{-1}) in the NOPC/PMS system depending on the electron transfer path with the necessity of moderate surfaced unpaired electrons for electrons delivery, which could be regulated by the modifier dosage. However, excessive surfaced unpaired electrons were unfavorable to PMS adsorption, resulting in deterioration of BPA degradation. This study indicates that controlling the amount of surfaced unpaired electrons in an appropriate range is essential to ensure the carbonaceous materials activity in PMS activation to obtain a satisfactory BPA degradation.

1. Introduction

Bisphenol A (BPA) as an industrial material widely applied for producing epoxyresins, polyacrylate and polycarbonate plastics has been ubiquitously detected in different aquatic environments [1,2]. Due to the potentiality of BPA to disrupt endocrine function [3], it is urgent to developing technologies for its efficient removal. Advanced oxidation processes (AOPs) as characterized by the production of reactive oxygen species (ROS) by activation of ozone [4], sulfite [5], H_2O_2 [6], peroxymonosulfate (PMS) [7–9], peroxydisulfate (PDS) [10–12], etc., have been generally applied to degrade refractory contaminants in wastewater such as BPA. Among them, PMS is the easiest to be activated due to the instability of its O-O bond arising from the asymmetric structure [13]. Numerous studies have focused on applying PMS-based AOPs for BPA removal, such as PMS/UV-C system [14] and Co^{2+}/PMS/UV system [15]. However, the demands of high energy input and the unsatisfactory efficiency make these activation methods inapplicable for the large-scale remediation. Transition metal catalysts are able to activate PMS effectively whereas the dissolved metal ions will pose new risks to environment [16,17]. Carbonaceous materials own advantages such as cost-effective, tunable electronic properties and environmental friendliness, promoting the application prospects for activating PMS [18].

g-C_3N_4 is an increasingly investigated covalent compound with a layered structure similar to graphene (Fig. S1) [19]. The characteristics of layered structure and rich nitrogen element make it an ideal precursor of for synthesizing N-doped graphene-like carbon materials [20,21]. Modification with N doping is able to increase the content of graphitic N, which has good electron delivery ability and catalytic activity [22]. Moreover, the modifiers of g-C_3N_4 are oxalic acid, mannitol, ascorbic acid and other oxygen-containing compounds generally, leading to the

* Corresponding authors at: State Key Laboratory of Hydraulics and Mountain River Engineering, College of Architecture and Environment, Sichuan University, Chengdu 610065, China.
E-mail addresses: hecs@scu.edu.cn (C.-S. He), laibo@scu.edu.cn (B. Lai).

https://doi.org/10.1016/j.apcatb.2022.121390
Received 23 November 2021; Received in revised form 5 April 2022; Accepted 6 April 2022
Available online 9 April 2022

inevitable containing of doped O atoms in the products derived from g-C_3N_4 [23,24]. Therefore, nonmetal heteroatoms doping is expected to boost the catalytic activity of carbon material.

As stated recently, the mechanism of PMS activation by nonmetal heteroatoms (e.g., C, N, O) doping in the matrix of g-C_3N_4 or carbonaceous materials was due to the production and oxidation effect of $^1O_2$ [23,25–27]. In those studies, the generation of $^1O_2$ was usually proved by electron paramagnetic resonance (EPR) tests and the contribution of $^1O_2$ to BPA degradation is proved by quenching experiments. However, those methods have some inherent drawbacks. For example, the inhibition of BPA degradation in the quenching tests may be due to the consumption of PMS by quencher rather than the scavenging of $^1O_2$ [28]. Furthermore, the possibility of $^1O_2$ to degrade pollutants in aqueous solution is limited by the rapid reaction between $^1O_2$ and H_2O [28]. Meanwhile, non-radical electron transfer pathway has been recently proposed to be responsible for phenolic compounds and some pharmaceuticals oxidation in persulfate system activated by carbonaceous materials like graphitic nano-diamond and carbon nanotubes via the introduction of in-situ Raman and electrochemical characterizations [29,30]. Therefore, the authentic contribution of $^1O_2$ in heteroatoms doping catalysts/PMS systems needs to be further verified, and a re-visit to the degradation mechanism of BPA in PMS/heteroatom doping carbonaceous system with careful exploration is necessary.

During the modification process, the losing of N atoms in g-C_3N_4 introduced the N vacancies. The C atoms around N vacancy would generate unpaired electrons due to the breaking of C-N bonds, which has also been expressed as 'Persistent Free Radical' in some studies [31–33]. Previous researches have confirmed the existence of unpaired electrons in manifold carbon-based materials by EPR spectroscopy. They directly drew a conclusion that the unpaired electrons were beneficial for the activity of carbonaceous catalysts regarding activating PMS but without deep exploration the underlying effect of unpaired electrons [34,35]. Therefore, it is urgent to gain deep insights into the effect of unpaired electrons of carbon-based catalysts on PMS activation.

Herein, a N and O co-doped carbon material with porous structure (NOPC) was prepared by simple pyrolysis. The elementary composition, morphology, microstructure, and electronic properties of NOPC were thoroughly analyzed and characterized. Furthermore, the mechanism of PMS/NOPC system for degrading BPA was carefully investigated by substantial experiments: unpaired electrons detection, premixing of NOPC and PMS, identification of ROS. More importantly, electrochemical characterization, EPR detection, PMS adsorption experiments, and density functional theory (DFT) analysis were applied to investigate surfaced unpaired electron influence on BPA degradation process. Finally, the possible degradation pathways of BPA in PMS/NOPC system were proposed according to the degradation intermediates detected by high performance liquid chromatography time-of-flight premier mass spectrometry (HPLC-QTOF-MS/MS).

2. Experiment section

2.1. Chemicals

BPA, urea, mannitol, sodium hydroxide, sodium thiosulfate, sulfuric acid, sodium sulfate, humic acid (HA), p-benzoquinone (BQ), ethyl alcohol (EtOH), tert-butanol (TBA), p-hydroxybenzoic acid (BA), potassium chloride, dimethyl sulfoxide (DMSO), and potassium dihydrogen sulfate were purchased from ChengDu Chron Chemicals Co. Ltd. (China). 2,2,6,6-tetramethyl-4-Piperidinol (TEMP, 98.0%), PMS, L-Histidine (99.5%), and 5,5-Dimethyl-1-pyrroline N-oxide (DMPO, 97.0%) were acquired from Aladdin reagent Inc (Shanghai, China). Methanol was obtained from Merck KGaA, Germany. Analytical reagents were used in all involved experiments. Deionized water in the experiments was prepared by a water purifier. Tap water was obtained from the laboratory of West China Campus, Sichuan University. Pond water and river water were acquired from the natural waters in Chengdu, Sichuan Province.

2.2. Catalysts preparation and NOPC regeneration

NOPC was prepared after modifying according to the methods described in the literature [23], as shown in Fig. S2. The precursor was obtained by fully grinding urea (10 g) and a certain amount of annitol individually followed with being placed in a 500 mL crucible. The crucible was heated to 550 °C at 2 °C/min in air and kept for 4 h. The calcined products were milled into powders and marked as NOPC-x, where "x" corresponds to the addition amount of mannitol (x = 1, 2, 3, 4, and 5 corresponding to 0.25, 0.5, 1.0, 1.5 and 2.0 g). Hereafter, NOPC-3 was abbreviated as NOPC. g-C_3N_4 was synthesized according to the similar procedure as NOPC-x but without the addition of mannitol. The modifier, mannitol, was directly calcined with similar procedure to prepare porous carbon (PC) as a control of NOPC. After 5 cycles, the used NOPC was collected by vacuum filtration and washed by deionized water, then dried in 60 °C. Finally, the used NOPC was recovered after calcination at 400 °C in N_2 atmosphere for 2 h.

2.3. Experimental procedures

150 mL of BPA stock solution (43.86 μM) was added into a 250 mL beaker to carry out the BPA degradation experiments. A water bath was used to keep the reactor temperature at 30 °C. The degradation process was initiated with the addition of catalyst (NOPC-x or pristine g-C_3N_4) and PMS into the reactor. The solution containing BPA and reagents was stirred by mechanical stirrer at 300 rpm. Quenching experiments were carried out by adding the corresponding quencher (EtOH, L-histidine, TBA, and BQ) into the reactor individually before the addition of catalyst and PMS. As for the NOPC stability test, the catalyst was collected through vacuum filtration after each reaction and then washed for three times by deionized water before their further addition into the reactor to start the next four cycles. During the reaction, samples were taken out for further filtration by a 0.22 μm polytetrafluoroethylene membrane at the predetermined time. These samples were injected into a vessel containing 45 μL $Na_2S_2O_3$ (0.1 M) to terminate the oxidation process. All experiments were operated at least twice to acquire average value and standard deviation.

For electrochemical characterization of catalyst, 5 mg NOPC was dispersed in 500 μL EtOH and 0.5 μL Nafion solution following 1 h of ultrasound. The 6 μL slurry was dipped on the glassy carbon electrode and dried with an infrared lamp. Open circuit potential (OCP) and time current curve (TCC) detections were conducted on the NOPC coated glassy carbon electrode with the addition of BPA or/and PMS. Na_2SO_4 (0.1 M) was the electrolyte in the above electrochemical experiments. Both the NOPC coated on the glassy carbon electrode and electrolyte was replaced by new prepared ones for each test. According to previous study, an electrochemical cell experiment was designed to investigate the contribution of electron transport path in PMS/NOPC system for BPA removal (Fig. S3) [36]. Briefly, the electrochemical cell consisted of two 250 mL beakers connected by copper wires attaching to electrodes (Fig. S3). The NOPC-modified graphite electrodes were prepared by dripping the slurry on to the graphite electrodes and drying naturally. A glass-U-tube filled with agarose gel containing saturated potassium chloride was used as a salt bridge to connect the two beakers to obtain a closed circuit. 150 mL 21.93 μM BPA and 1.5 mM PMS solution was added to the anodic and cathodic cell, respectively. The solution in the beakers was stirred by magnetic stirrer during the reaction.

As for Fourier Transform Infrared Spectrometer (FTIR) spectra, samples were thoroughly ground with KBr to prepare thin films for detection by Nicolet 6700 FTIR spectrometer at a resolution of 4 cm^{-1}. The experiment of radical detection took place in a 10 mL PVC tube which contained 8 mL purified water and trapping agent. The reaction was initiated by adding the catalyst and oxidant rapidly. After 30 s of full oscillation, solution was filtered to be further detected by EPR

spectrometer within 5 min

2.4. Analytical methods

The residual BPA was detected by high performance liquid chromatography (HPLC, Shimadzu, Japan) with an Eclipse XDB C-18 column, whose temperature was stabilized at 30 °C. A mixture of water (A) and methanol (B) in a certain volume ratio (A: B= 20%:80%) was used as the mobile phase of HPLC at 0.8 mL/min. The characteristic absorbance wavelength of BPA was 230 nm. Total organic carbon (TOC) of the effluent in different system was detected by TOC analyzer (Shimazu, Japan). EPR analysis was explored on a Bruker EMX plus X-band CW EPR spectrometer (Germany) to identify the radicals generated in PMS/NOPC-x systems and detect the relative content of unpaired electrons concentration contained in each NOPC-x. The deionized water used in EPR detection of $^1O_2$ was boiled to exclude the effect of oxygen molecules. The dosage of NOPC-x was equal during unpaired electrons concentration detections by EPR to ensure comparability of signal intensity of each sample. According to former reports [31–33,35], the peak height of the signals in the Lorentzian lines was used to represent the relative number of unpaired electrons. The detection signal of EPR was fitted by spin-fit of Bruker.

The residual PMS was analyzed by an iodometry. Briefly, the liquid samples were taken out to mix with 0.5 M KI buffered with 0.07 M $NaHCO_3$ at the pre-designed interval. After standing for half an hour, the mixture was detected by a UV–vis spectrophotometer (UV1800, SHIMADZU) at 351 nm [8]. The intermediates of BPA were detected by UPLC-QTOF -MS/MS (Agilent 1290 infinity UPLC with Agilent G6564 Q-TOF Mass Spectrometer) equipped with Eclipse plus C18 column (Eclipse pluse-C18 3.0 × 100 mm 1.8 μm). Analysis details were provided in Table S1. The intermediates were detected by error and Double Bond Equivalent (DBE) discussions. The calculated DBE and *m/z* error were determined by Eq. (1) and Eq. (2), separately [37].

$$\text{Error} = (m/z_{\text{exact}} - m/z_{\text{calculated}})/\, m/z_{\text{exact}} \times 10^6 \quad (1)$$

$$\text{DBE} = \text{C} + 1 - \text{H}/2 \quad (2)$$

where C and H represented the number of carbon and hydrogen atoms respectively.

Fourier Transform Infrared Spectrometer (FTIR) spectra were obtained by Nicolet 6700 FTIR spectrometer (USA). Raman analysis was performed by confocal Raman spectrometer (Thermo Fisher Scientific, USA) with a 532 nm excitation wavelength. The electrochemical tests were conducted on a CHI 604E Electrochemical Workstation (CH Instrument Co., China) with a three-electrode system. The morphology of g-C_3N_4 and NOPC was photographed via scanning electron microscope (SEM-EDS, SU-8010, Hitachi, Japan) and transmission electron microscopy (TEM, FEI Talos F200x, FEI Company, USA). X-ray diffraction (XRD) (PANalytical B.V., Holland) with CuKa radiation (40KV, 40 mV) was adopted to investigate the crystallographic structure of samples. 2θ data from 10° to 70° was collected with a 0.03 sampling pitch by a continuous scan at a 2° /min scan rate. The element composition of samples was identified by X-ray photoelectron spectroscopy (XPS) (AXIS Ultra DLD, Kratos Co., UK). The nitrogen adsorption and desorption curves were tested by Micromeritics ASAP 2460 (Micromeritics, USA) and the Brunauer-Emmett-Teller surface area (SA_{BET}) was analyzed by the Brunauer-Emmett-Teller model.

2.5. Kinetic studies and DFT calculation

Pseudo-first-order-model (Eq. (3)) was applied to analyze the BPA degradation, where C_0 means primal BPA concentration and C_t represents residual BPA after t minutes. k_{obs} is indicative of the pseudo-first-order kinetic rate constant of BPA degradation.

$$\ln\left(\frac{C_t}{C_0}\right) = -k_{\text{obs}} \times \text{t} \quad (3)$$

The Vienna Ab-initio Simulation Package (VASP 5.4) was applied to execute the first-principle calculation. The exchange and correlation of electron was calculated by the generalized gradient approximation functional (GGA-PBE). The electron–ion interaction was delineated by the projector-augmented wave (PAW). The k-point mesh was 3 × 3 × 1 and the cut-off energy was 400 eV. The energy and force converged to 10^{-5} eV/atom and 0.01 eV/Å in several. An 8 × 8 × 1 supercell of NOPC was established in a 15 Å vacuum gap. Eq. (4) is the calculate formula of PMS adsorption energy (*Eads*), where E_{PMS}, E_{NOPC}, and $E_{PMS/NOPC}$ represent the single PMS, NOPC, and the total energies of the PMS/NOPC system, in the same slab, separately [38].

$$E_{ads} = E_{NOPC/PMS} - (E_{PMS} + E_{NOPC}) \quad (4)$$

3. Results and discussion

3.1. Cost analysis and characterization of NOPC

The price and consumption of the raw materials for the preparing of NOPC were detailed in Table S2. Ignoring the cost of deionized water and power, and considering product yield of 5.55% (0.61 g), the production cost of NOPC was estimated to be about 0.11 $/g, which was lower than the cost of most other carbon-based catalysts (Table S2). Meanwhile, it is noteworthy that in large scale applications the final expenditures with raw materials to prepare NOPC would be lower than the calculated price here.

After adding mannitol during the pyrolysis process the product (NOPC) became loose and porous compared with g-C_3N_4 (Fig. 1(a)-(d)), which was also confirmed by the larger SA_{BET}, pore features of NOPC (Table S3). Table S3 shows that the content ratio of C to N improved from 0.72 in g-C_3N_4 to 1.3 in NOPC, indicating that a large number of N atoms lost during pyrolysis, which could result in N vacancies [31]. The EDS-mapping of NOPC (Fig. 1(e)-(h)) displays the even distribution of N, O and C elements.

As shown in Fig. S4(a) - (b), the diffraction peak appeared at 12.9° in the XRD pattern of NOPC and the peak located at 809 cm^{-1} in NOPC FTIR spectrum, both corresponding to typical heptazine, disappeared completely [20,23]. The above experiment results indicated that NOPC was not a typical g-C_3N_4 structure. As seen from Fig. S5(a)-(d), the intensity of the peak which was related to sp^2 hybridized C atoms of heptazine rings (N═C-N) reduced with the increase of 'x'. Meanwhile, the proportion of C-C/C═C increased from 26% to 59%, demonstrating that the structure of triazine rings in NOPC was destroyed [39,40]. The bands at 1349 and 1590 cm^{-1} of NOPC Raman spectra match to the D and G bands of graphite materials, suggesting the conversion of NOPC from g-C_3N_4 to N and O co-doped porous carbon (Fig. S4(c)) [41].

Previous studies have clarified that the graphitic N contained in the carbon-based materials might play a key role for PMS activation [42,43], since the graphitic N has a higher electronegativity and smaller atom radius to accelerate the electron transfer [44]. Therefore, we explored the relative contents of different N species contained in g-C_3N_4 and NOPC by XPS analyses [34,45]. The proportion of graphitic N in NOPC-x increased with the increase of the dosage of mannitol (Fig. 2 (a)-(d)), which was beneficial for electron transfer in NOPC-x [46,47]. As shown in Fig. 2(e), the semicircle diameter in the Nyquist plots of g-C_3N_4 and NOPC-x decreased with the increase of modifier dosage as shorter semicircle diameter indicated the lower electronic resistance [48]. Meanwhile, the corrosion currents of NOPC-x calculated from Tafel slope enhanced with the amounts of unpaired electrons (Fig. 2(f) and Table S4). The above discussions indicate that the unpaired electrons could heighten the electron conductivity of NOPC-x [49,50].

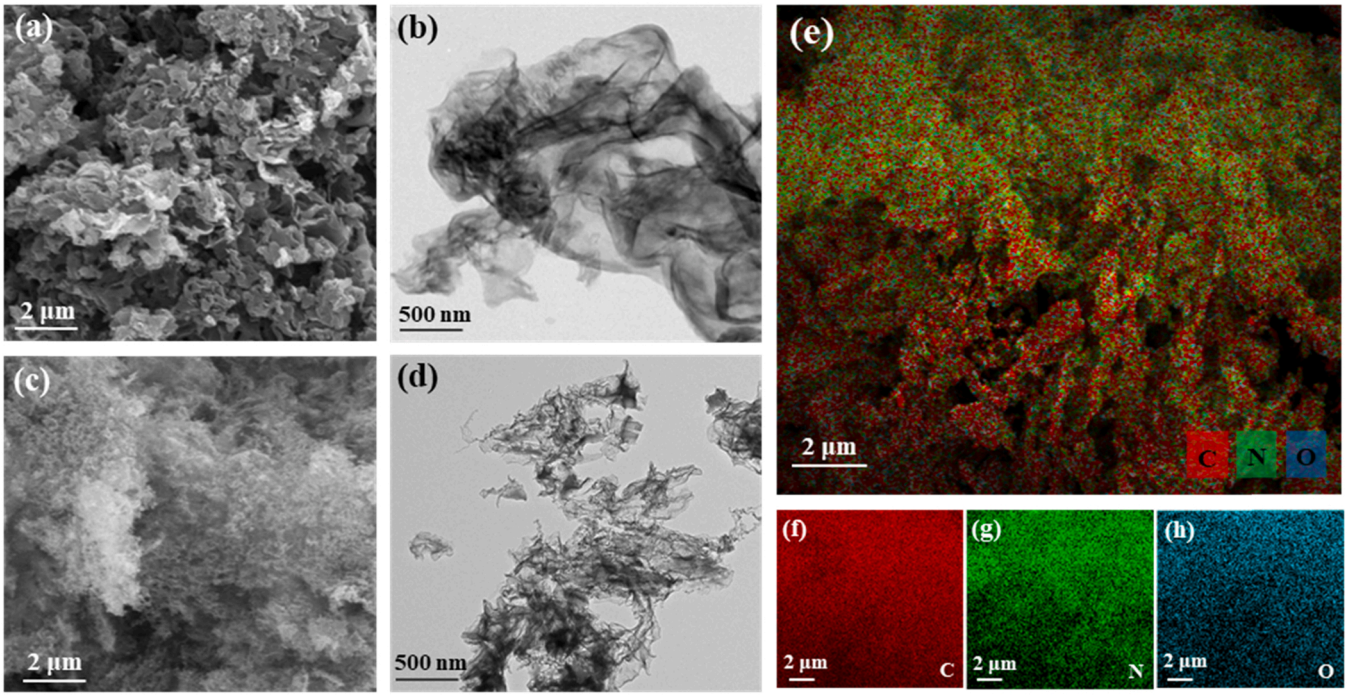

Fig. 1. Morphology and component analysis of g-C_3N_4: (a) SEM, (b) TEM, and of NOPC: SEM (c), TEM (d), and EDS-mapping of NOPC: (e)-(h).

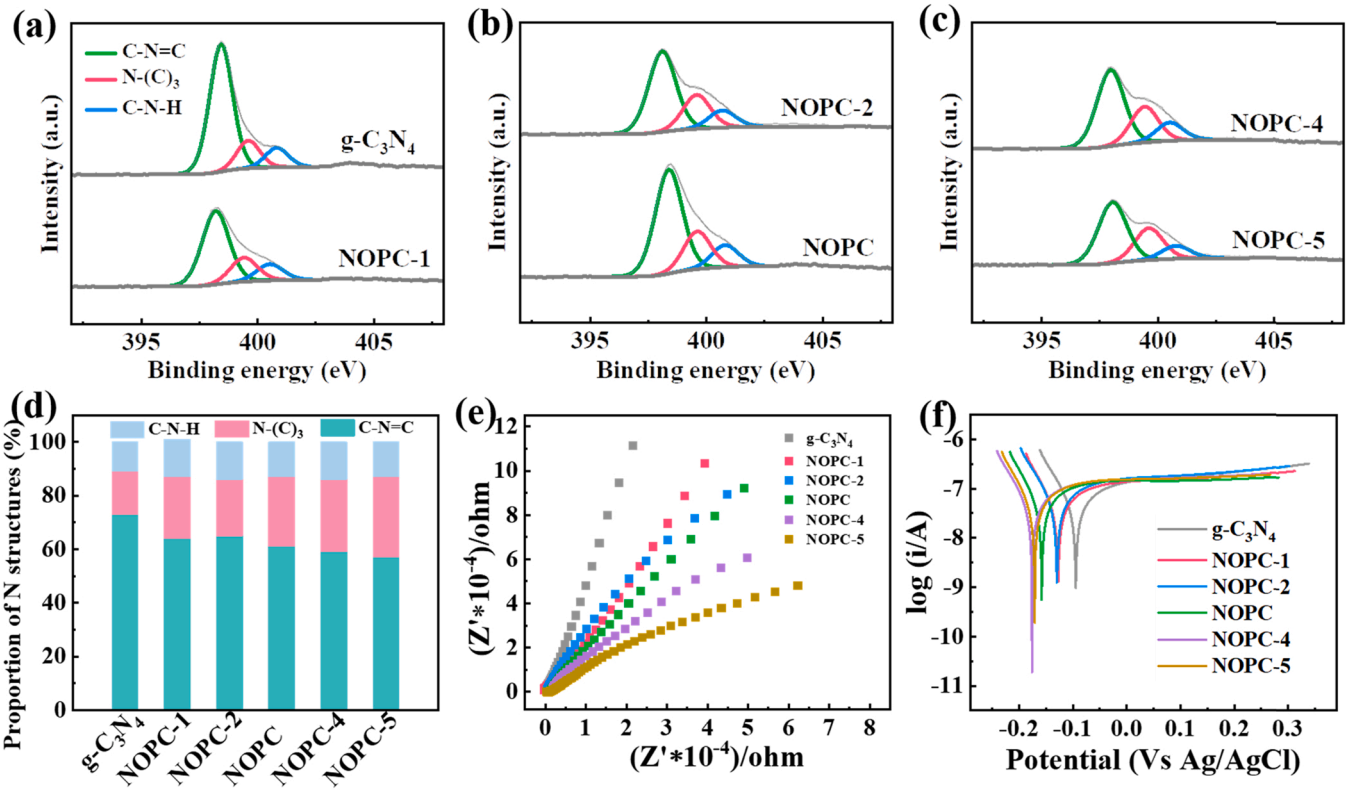

Fig. 2. XPS spectra (a)-(c), N species content (d), Nyquist plots (e) and Tafel curve analysis (f) of g-C_3N_4 and NOPC-x.

3.2. Catalytic activity of NOPC

3.2.1. Control experiments

The efficiencies of BPA removal were investigated in four systems (i.e., PMS alone, NOPC alone, PMS/NOPC, g-C_3N_4/PMS). As shown in Fig. 3(a)-(b), trace BPA was adsorbed by NOPC or g-C_3N_4, indicating that neither NOPC nor g-C_3N_4 possessed adsorption effect on BPA. The removal efficiency of BPA in 20 min and the pseudo first-order reaction kinetics in PMS alone (1.53%, 0.0044 min^{-1}) were far below than those in PMS/NOPC system (100%, 0.30 min^{-1}), indicating that the PMS couldn't oxidize BPA directly. Therefore, the BPA was removed via other ways in NOPC/PMS system. Moreover, according to Fig. S6, the BPA

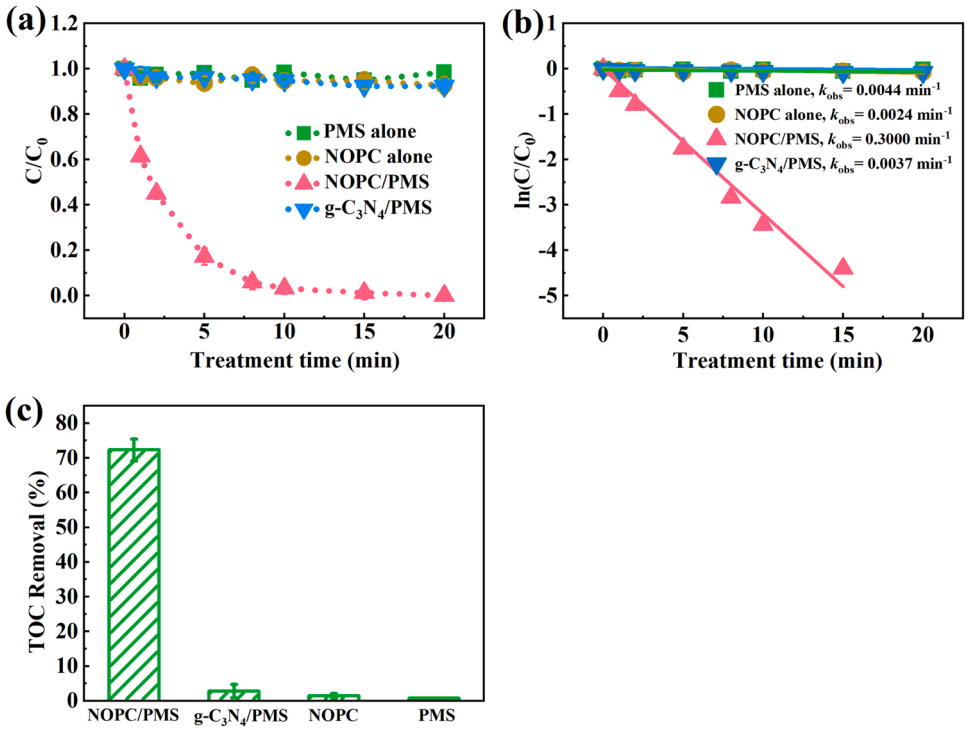

Fig. 3. BPA degradation (a), k_{obs} (b), and TOC removal (c) in PMS alone, NOPC alone, PMS/NOPC, and g-C_3N_4/PMS systems ($[BPA]_0 = 43.86$ μM, $[NOPC]_0 = 0.2$ g/L, $[PMS]_0 = 0.15$ mM, $pH_0 = 6.6$).

removal efficiency in NOPC/PMS system was apparently higher than that of PC/PMS system. Meanwhile, Table S5 summarized relevant researches about PMS activation by carbon-based catalysts, which further indicated the outstanding catalytic activity of NOPC comprehensively considered from efficiency and the dosage of catalyst and PMS.

The difference between TOC_{BPA} (7.68 mg/L) and $TOC_{BPA/NOPC}$ (7.59 mg/L) was tiny, excluding the influence of the dissolved organic matter (DOM) dissolved from NOPC on TOC removal. Meanwhile, as partially contributed by the adsorption of intermediate products of BPA degradation onto NOPC, 72.30% TOC removal of BPA was achieved in PMS/NOPC system within 20 min, demonstrating the outstanding catalytic activity of NOPC (Fig. 3(c)) [25]. These results indicated that NOPC exhibited remarkable catalytic activity for PMS towards BPA removal, probably a result of their higher SA_{BET} and graphitic N proportion compared with g-C_3N_4. Large surface area and adequate pores benefited the mass transfer between the catalysts and PMS, as well as high graphitic N ratio is favorable to electrons transport [25].

3.2.2. The effect of experiment conditions

As displayed in Fig. S7(a)-(d), both the final BPA removal and the k_{obs} of BPA degradation were expectedly enhanced with the increase in the dosage of PMS and/or NOPC due to more contact sites for PMS and BPA, and the increase in electron acceptors, respectively.

Fig. S8(a)-(b) revealed that BPA can be totally degraded in PMS/NOPC system at both acidic and neutral conditions (3.0–6.6) within 20 min. According to the dissociation constants of BPA ($pK_{a1} = 9.6$, $pK_{a2} = 10.2$) and PMS ($pK_{a1} < 0.0$, $pK_{a2} = 9.4$), zero-point charge of NOPC ($pH_{zpc} = 3.1$, calculated from Fig. S8(c)), the charged situation of three reactants were summarized in Table S6 with different initial pH [51,52]. When the pH of the solution was 3.0, NOPC, BPA, and PMS can freely interact with each other due to the absence of electrostatic repulsion between them, resulting in the highest BPA removal efficiency. However, due to the intense repulsion between the negative charges carried by BPA ($Bis(O)^{2-}$), NOPC, and PMS (HSO_5^- or SO_5^{2-}), BPA removal was severely inhibited when the initial pH was 9.0 or 11.0.

As the solution contained 50 μM of Cl^- or $H_2PO_4^-$, the BPA removal efficiency reached at 100% and 92.0% severally within 20 min, suggesting that the inorganic anions commonly contained in natural waterbody hardly weaken the ability of PMS/NOPC system for the removal of BPA (Fig. S8(d)). After adding 50 μmol-C/L of HA to the PMS/NOPC system, the BPA degradation efficiency reduced from 100% to 94.0%, which might arise from the block of contact between BPA and NOPC by HA. Besides, the PMS/NOPC system exhibited satisfactory BPA removal in real water matrixes. As shown in Fig. S8(e), BPA could be completely removed by PMS/NOPC system in tap water. Meanwhile, the final BPA removal efficiency within 20 min was about 90% and 80% in pond water and river water, respectively, indicating that the PMS/NOPC system has practical significance for the environmental remediation.

3.2.3. The stability of NOPC

BPA degradation efficiency in PMS/NOPC system decreased from 100% to 80.61% after 5 cycles, indicating the reduced performance of NOPC after reuse (Fig. S9). The adsorption capacity of fresh NOPC, used NOPC, and regenerative NOPC for PMS was identified to explore the reason for the decrease of NOPC catalytic activity. As shown in Fig. S10, the adsorption capacity of NOPC for PMS decreased significantly after using for 5 times, which might arise from the adsorption of degradation intermediates on the surface of NOPC to block the active sites [37] However, it should be noted that the adsorption capacity and catalytic activity of the used NOPC could be completely regenerated by calcination at 400 °C in N_2 atmosphere for 2 h, resulting from the removal of the surface adsorbed degradation products as illustrated in Fig. S10.

3.3. Reaction mechanisms of PMS/NOPC system

3.3.1. Contribution of radicals

An in-depth study on ROS that might contribute to BPA degradation was conducted to identify the generation of ROS in PMS/NOPC system. It is well documented that HO• usually makes an important contribution to the degradation of pollutants in PMS-activated systems [7,53]. The contribution of HO• could be evaluated by adding excess TBA to quench HO• ($k = 6.0 \times 10^8$ $M^{-1}s^{-1}$) selectively [54]. However, Fig. 4(a)

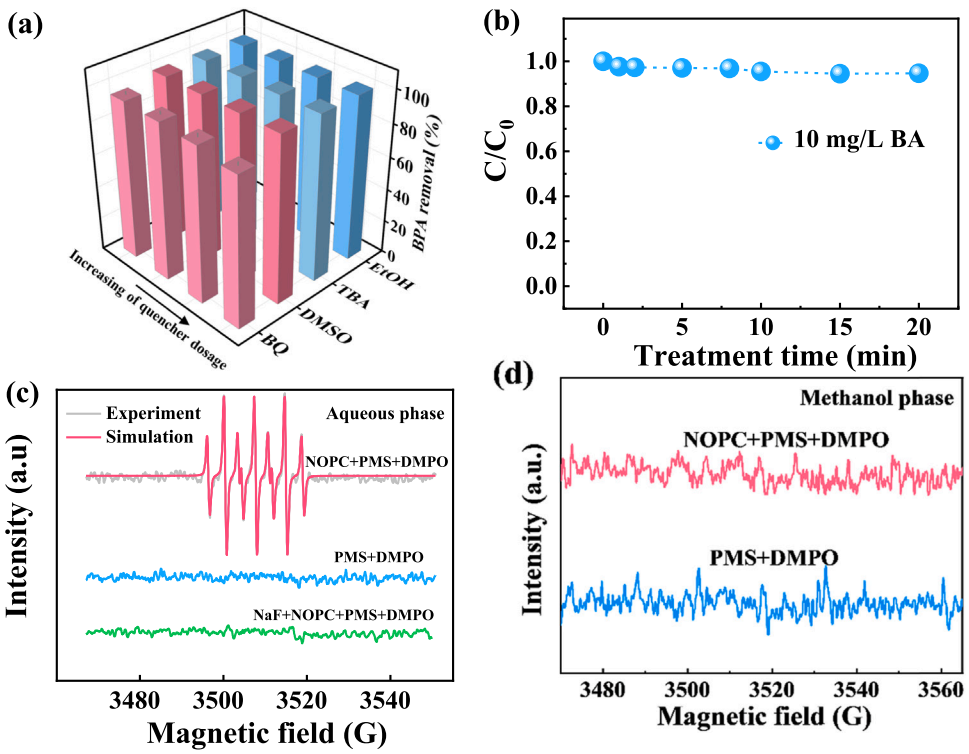

Fig. 4. Effects of four quenchers on BPA degradation in PMS/NOPC system (the quencher dosage increased with the direction of the black arrow, $[BPA]_0$ = 43.86 μM, $[NOPC]_0$ = 0.2 g/L, $[PMS]_0$ = 0.15 mM, $[EtOH]_0$ = 200, 300, 400, 500 mM, $[TBA]_0$ = 200, 300, 400, 500 mM, $[DMSO]_0$ = 5, 10, 15, 20 mM, $[BQ]_0$ = 1, 2, 5,10 mM) (a); the degradation of BA in PMS/NOPC system ($[NOPC]_0$ = 0.2 g/L, $[PMS]_0$ = 0.15 mM) (b); EPR detection results of PMS/NOPC system in different media (c)-(d) ($[NOPC]_0$ = 1.0 g/L, $[PMS]_0$ = 0.75 mM, $[DMPO]_0$ = 40 mM, [NaF]= 5 mM, pH_0 = 6.6).

indicated that excessive TBA didn't reduce the degradation of BPA at all even though the dosage of TBA was 500 mM, demonstrating that HO• didn't contribute to BPA removal in PMS/NOPC system. Degradation experiment of BA ($k_{(BA,\ HO\bullet)} = 4.2 \times 10^9\ M^{-1}s^{-1}$) in PMS/NOPC system was carried out to further explore the existence of HO• [55,56]. Obviously, PMS/NOPC process couldn't degrade BA effectively (Fig. 4(b)), indicating that little HO• was might generated during the oxidation process. In order to further verify the above conclusion, we applied EPR technology to identify the existence free radicals in the PMS/NOPC system. As shown in Fig. 4(c), the stimulation result of the EPR signal fitted the spectrum of DMPO-x very well, which was resulted from the oxidation of DMPO. Meanwhile, no signal of DMPO-HO• was detected in NOPC/PMS/DMPO system with different dosage of DMPO, indicating no generation of HO• in NOPC/PMS system (Fig. 11(a)).

$SO_4^{\bullet-}$ as another common free radical has been found to account for pollutants degradation in most PMS-activated systems [13,57]. However, BPA removal efficiency was not inhibited by the addition of 200–500 mM EtOH (as $SO_4^{\bullet-}$ scavenger) in NOPC/PMS system, manifesting that $SO_4^{\bullet-}$ didn't contribute to the BPA removal (Fig. 4(a)). Meanwhile, BA ($k_{(BA,\ SO4\bullet-)} = 2.5 \times 10^9\ M^{-1}s^{-1}$) could be degraded efficiently in the presence of $SO_4^{\bullet-}$ due to their high second order kinetic constants [53,57]. Whereas, Fig. 4(b) shows that the removal of BA was extremely limited, implying the absence of $SO_4^{\bullet-}$ in NOPC/PMS system. Furthermore, no signal of DMPO-$SO_4^{\bullet-}$ appeared in the EPR spectra with different dosage of DMPO, which further excluded the existence of $SO_4^{\bullet-}$ in NOPC/PMS system (Fig. 4(c) and Fig. S11(a)).

The surface bonded radicals were identified by considering their responses to the addition of DMSO, which could quench the surfaced ROS [58]. Fig. 4(a) shows that the BPA removal wasn't impaired by the addition of DMSO even though the dosage increased from 5 to 20 mM, indicating that surfaced sulfate or hydroxyl radicals didn't contribute to BPA removal. Moreover, since F^- can desorb surface radicals bonded to the catalyst by forming hydrogen bond, the EPR test after adding NaF was conducted to identify the existence of surfaced sulfate or hydroxyl radicals [59]. As illustrated in Fig. 4(c) and Fig. S11(b), no signal of radicals emerged with the addition of different dosage of NaF, suggesting that no surfaced sulfate or hydroxyl radicals were contained in the obtained NOPC. It has been reported that $O_2^{\bullet-}$ is also frequently detected in PMS-activated systems [60]. In this study, BQ was applied to quench the suspected $O_2^{\bullet-}$ due to the selective reaction between them ($k_{(BQ,\ O2\bullet-)} = (0.9–1.0) \times 10^9\ M^{-1}s^{-1}$) [60]. As shown in Fig. 4(a), the final BPA removal efficiency in PMS/NOPC system decreased from 100% to 95.8% when dosage of BQ was 1 mM, and decreased to 90.1% with the addition of 5 mM BQ addition, indicating the insignificant contribution of $O_2^{\bullet-}$ to BPA removal. Furthermore, formation of $O_2^{\bullet-}$ was examined by EPR spin-trapping techniques in methanol media, since the facile disproportionation reaction between $O_2^{\bullet-}$ and H_2O would prevent the trapping of $O_2^{\bullet-}$ by DMPO [61,62]. No signal of $O_2^{\bullet-}$ emerged in EPR spectra with different dosage of DMPO implied the absence of $O_2^{\bullet-}$ in PMS/NOPC system (Fig. 4(d) and Fig. S11(c)).

According to above analyses, the contribution of HO•, $SO_4^{\bullet-}$ and $O_2^{\bullet-}$ in PMS/NOPC system to BPA degradation could be ignored. There would be other reaction mechanisms rather than the above radicals mediated pathways responsible for BPA removal in PMS/NOPC system.

3.3.2. *Contribution of nonradical reactions*

3.3.2.1. Contribution of $^1O_2$. Researchers have proposed that $^1O_2$ could effectively degrade BPA contained in water via using L-histidine as quencher ($k_{(L\text{-histidine},\ 1O2)} = (2.4–3) \times 10^9\ M^{-1}S^{-1}$) in the oxidation systems [25,63]. However, the L-histidine quenching method has been challenged since L-histidine not only reacts with $^1O_2$, but also rapidly consumes PMS [64]. In this study, the final BPA degradation efficiency decreased sharply from 100% to 26.5% with the addition of 2 mM of L-histidine. However, L-histidine consumed 60% PMS within 2.5 min due to the reducibility of it (Fig. 5(a)) [64,65]. Obviously, the extra consumption of PMS would inevitably reduce the final removal of BPA. As such, the L-histidine quenching experiment couldn't properly identify the generation and contribution of $^1O_2$ in PMS/NOPC system. Fig. 6.

This study applied EPR to verify whether $^1O_2$ was generated during the oxidation process. Apparent three-line signals (a_N = 16.9 G) were detected in the EPR spectra of all systems (PMS alone, NOPC-1/PMS,

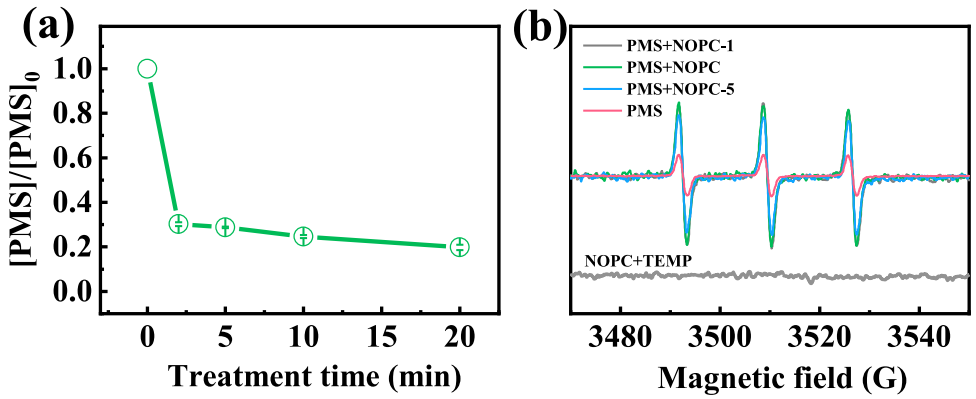

Fig. 5. The consumption efficiency of PMS with addition of L-Histidine (a); three-line signals of EPR spectra in five systems (b) ($[BPA]_0$ = 43.86 μM, $[NOPC]_0$ = 0.2 g/L, $[PMS]_0$ = 0.15 mM, $[L\text{-}Histidine]_0$ = 25 mM, $[TEMP]_0$ = 20 mM, pH_0 = 6.6).

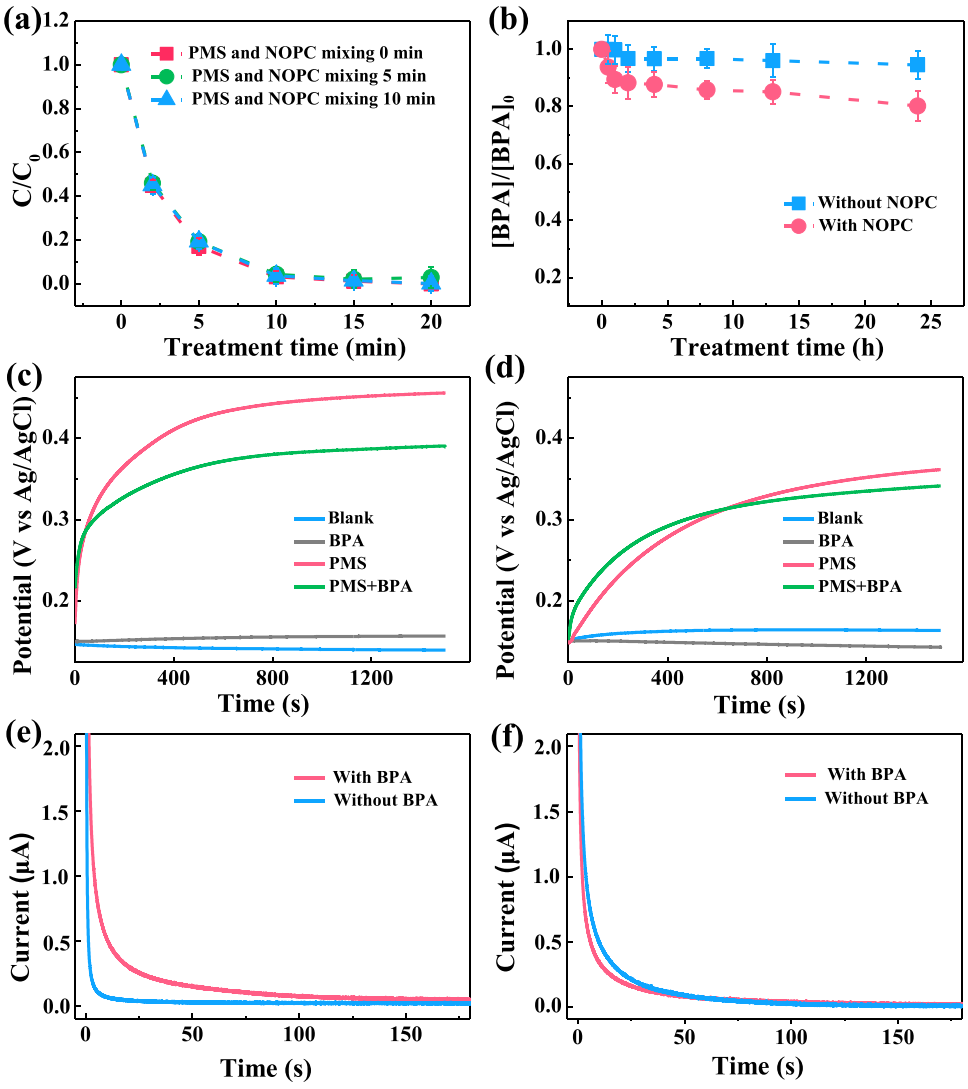

Fig. 6. The effect of NOPC and PMS premixing on BPA degradation (a) ($[BPA]_0$ = 43.86 μM, $[NOPC]_0$ = 0.2 g/L, $[PMS]_0$ = 0.15 mM, pH_0 = 6.6); BPA removal in electrochemical cell experiments (b) ($[BPA]_0$ = 21.93 μM, $[PMS]_0$ = 1.5 mM, pH_0 = 6.6); OCP changes in the addition of PMS or/and BPA monitored on the NOPC modified working electrode (c) and on the bare working electrode (d) ($[BPA]_0$ = 219.30 μM, $[PMS]_0$ = 1.5 mM, pH_0 = 6.6); TCC with or without BPA monitored on the NOPC modified working electrode (e) and on the bare working electrode (f) ($[BPA]_0$ = 219.30 μM, $[PMS]_0$ = 1.5 mM).

PMS/NOPC and NOPC-5/PMS) (Fig. 5(b)) [27]. Simultaneously, the signals were detected with different dosage of TEMP in anoxic aqueous phase regardless the addition or absence of NOPC (Fig. S11(d)), manifesting that the three-line signals were the oxidative products of TEMP by $^1O_2$ but not oxygen molecules [66,67]. Notably, the TEMP-$^1O_2$ signal intensity of NOPC-1/PMS, PMS/NOPC and NOPC-5/PMS was consistent, indicating that the production of $^1O_2$ in the three systems was similar [68]]. However, it's worth noting that there were significant differences between the ability of the three systems to degrade BPA (Fig. 7(b)-(c)). The reaction solution became alkaline with 20 mM TEMP (spin trapping agent) and PMS was activated by base to generate $^1O_2$ (Eqs. (5)–(6)) [13,69]. Therefore, TEMP-$^1O_2$ signals were also detected

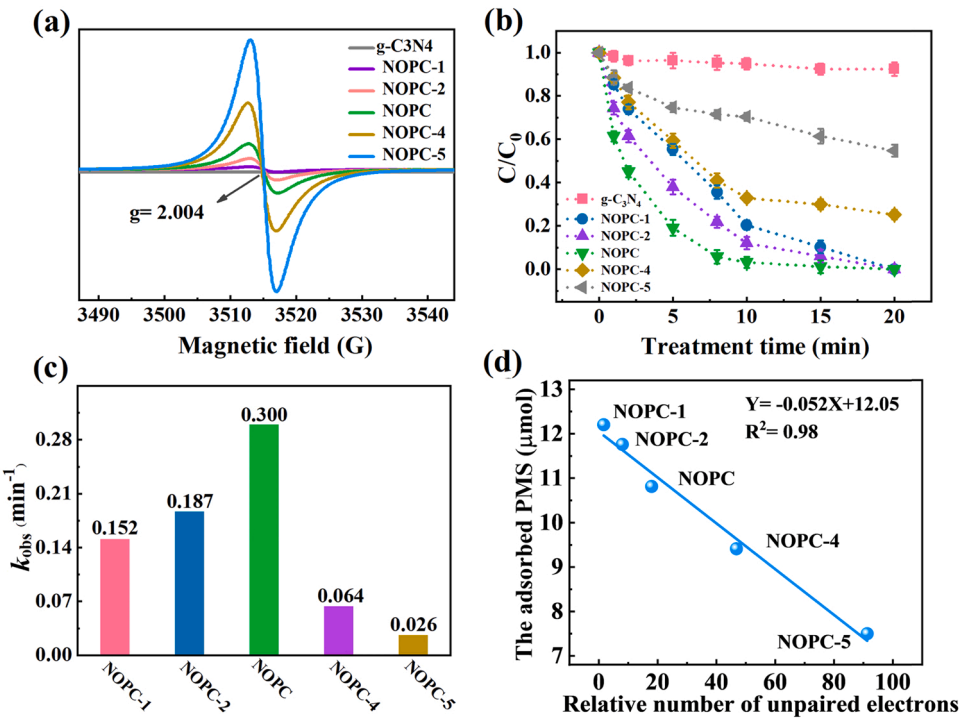

Fig. 7. EPR detection results of unpaired electrons of g-C_3N_4 and various NOPC-x (a); the BPA removal in different systems (b)-(c); the correlation between the relative amount of unpaired electrons on NOPC-x surface and the adsorption of PMS (d) ($[BPA]_0$ = 43.86 μM, $[NOPC]_0$ = 0.2 g/L, $[PMS]_0$ = 0.15 mM, pH_0 = 6.6).

in PMS alone systems (Fig. 5(b) and Fig. S11(d)). Nevertheless, the PMS alone system could hardly degrade BPA (Fig. 3a). These experimental results indicated that the $^1O_2$ was indeed generated in the above-mentioned systems, whereas the production of $^1O_2$ was not large enough to effectively degrade BPA in PMS/NOPC system.

$$HSO_5^- \rightarrow H^+ + SO_5^{2-} \quad (5)$$

$$HSO_5^- + SO_5^{2-} \rightarrow HSO_4^- + SO_4^{2-} + {}^1O_2 \quad (6)$$

3.3.2.2. Contribution of electron-transfer effect. Recently, a new non-radical electron transfer mechanism in the persulfate (PMS or PDS) activation by carbon-based materials systems has been proposed in several studies [29,30,43,70]. After the possible contribution of active radicals and $^1O_2$ towards BPA degradation was gradually excluded, the premixing experiment of NOPC and PMS was carried out here to check whether there was an electron transfer mechanism in PMS/NOPC system as reported previously. The removal of BPA didn't be affected after the premixing of NOPC and PMS for 5 or 10 mins, suggesting that the PMS/NOPC system was likely to degrade BPA directly through electron transfer process (Fig. 6(a)) [68]. Electrochemical cell experiment was further conducted to verify the above hypothesis. In electrochemical cell experiments, the BPA concentration decreased by 4.39 μM when the graphite electrode was modified with NOPC, while only 1.32 μM BPA was reduced using bare electrode ((Fig. 6(b)).

The experimental results indicated that NOPC strengthened the electron transfer from PMS/NOPC to BPA [36]. To verify the role of NOPC in promoting electron transfer, the OCP and TCC of PMS/NOPC system with the NOPC modified or bare working electrode were measured. When the working electrode was coated with NOPC, the OCP rose sharply to 0.456 V after PMS was added to the electrolyte (Fig. 6 (c)), which was due to the generation of a NOPC-PMS complex with strong oxidizing property [30]. The OCP increased and stabilized at 0.390 V (less than 0.456 V) with the co-addition of BPA and PMS because the NOPC-PMS complex was reduced by BPA. However, the addition of PMS would only enhance the OCP to 0.362 V if no NOPC was coated on the working electrode. Simultaneously, no significant difference existed in the value of OCP between the addition of PMS and co-addition of BPA and PMS, which was because that no active NOPC-PMS complex could be formed without NOPC (Fig. 6(d)).

As shown in Fig. 6(e), since BPA could work as an electron donor, the circuit current increased noticeably with NOPC coated on working electrode when BPA was added to the electrolyte. Conversely, the circuit current showed little change after addition of BPA with the bare working electrode owing to the lack of electron provider (Fig. 6(f)). The above results disclosed that nonradical electron-transfer was the main pathway responsible for BPA degradation in PMS/NOPC system.

According to the above analysis and results, a possible catalytic mechanism of PMS/NOPC system for BPA degradation was proposed (Scheme 1). PMS was activated by NOPC to generate a small amount of $^1O_2$, which made a limited contribute to the removal of BPA. Additionally, BPA could directly transfer electrons to PMS through NOPC with good electrical conductivity, achieving effective BPA degradation.

3.4. Effects of unpaired electrons on the degradation of BPA

As reported previously, the removal of N atoms in graphene-like structure would lead to the appearance of unpaired electrons on C atoms [31,32], which was beneficial for the electron transfer [35,50]. Herein, the unpaired electrons of NOPC-x and g-C_3N_4 were characterized via EPR analysis. A single Lorentzian line which was centered at a g value of 2.004 belongs to the unpaired electrons on C atoms result from the broken of C-N bonds [31,32]. The intensity of Lorentzian lines is positively correlated with the number of unpaired electrons.

As illustrated in Fig. 7(a), the intensity of Lorentzian lines of NOPC-x improved with the increase of "x", demonstrating the enhancement of NOPC-x unpaired electrons amount. This phenomenon might arise from the generation of more vacancies induced by the increasing modifier dosage. DFT calculation was further conducted to confirm the above conclusion. Top view and side view of NOPC-x models before optimization and the PMS adsorption model after optimization are listed in

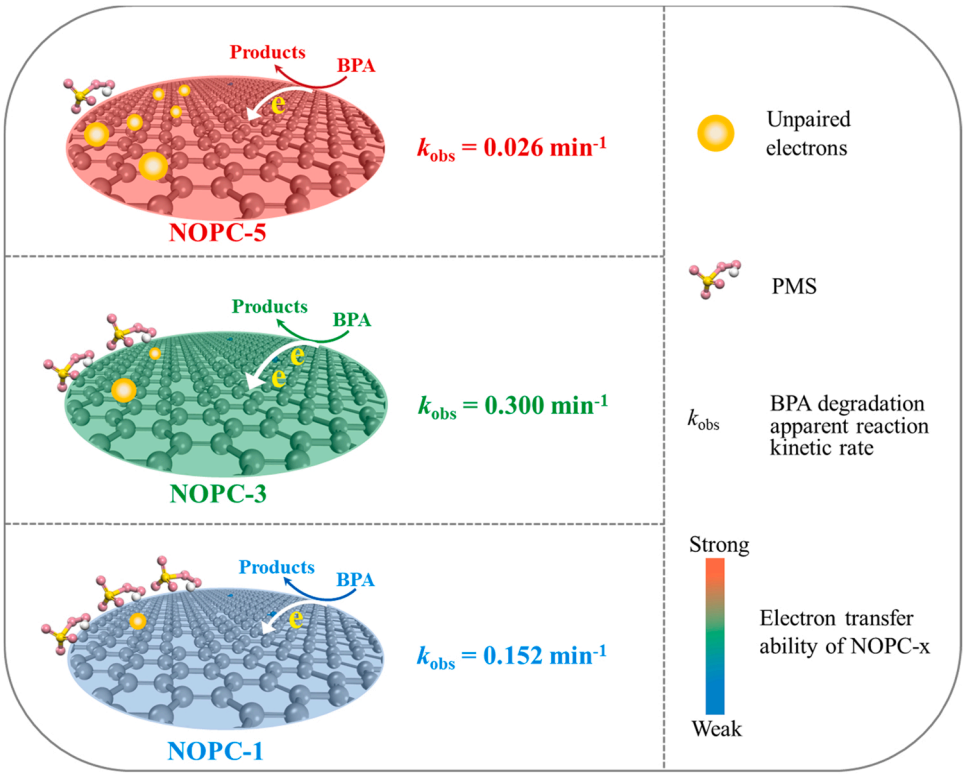

Scheme 1. Schematic illustration of BPA degradation mechanism in PMS/NOPC-x system by electron transport pathway.

Table S7. Electrostatic potential (ESP) distributions of three models are illustrated in Fig. 8(a), in which the blue and yellow area represents electron lacking and electron enrichment, respectively. Clearly, more unpaired electrons were formed on the NOPC surface with the increase of modifier dosage. The amount of unpaired electrons on the surface of NOPC-x remained essentially unchanged before and after the reaction referring to EPR detection results (Fig. S12). Meanwhile, $SO_4^{\bullet -}$ and HO•, the typical products derived from PMS activation, were not detected in NOPC/PMS system (Fig. 4(c)), indirectly demonstrating that the unpaired electrons could not activate PMS to degrade BPA.

According to EPR detections and electrochemical characterizations results (Fig. 7(a), Fig. 2(e)-(f), Table S4), both the unpaired electron

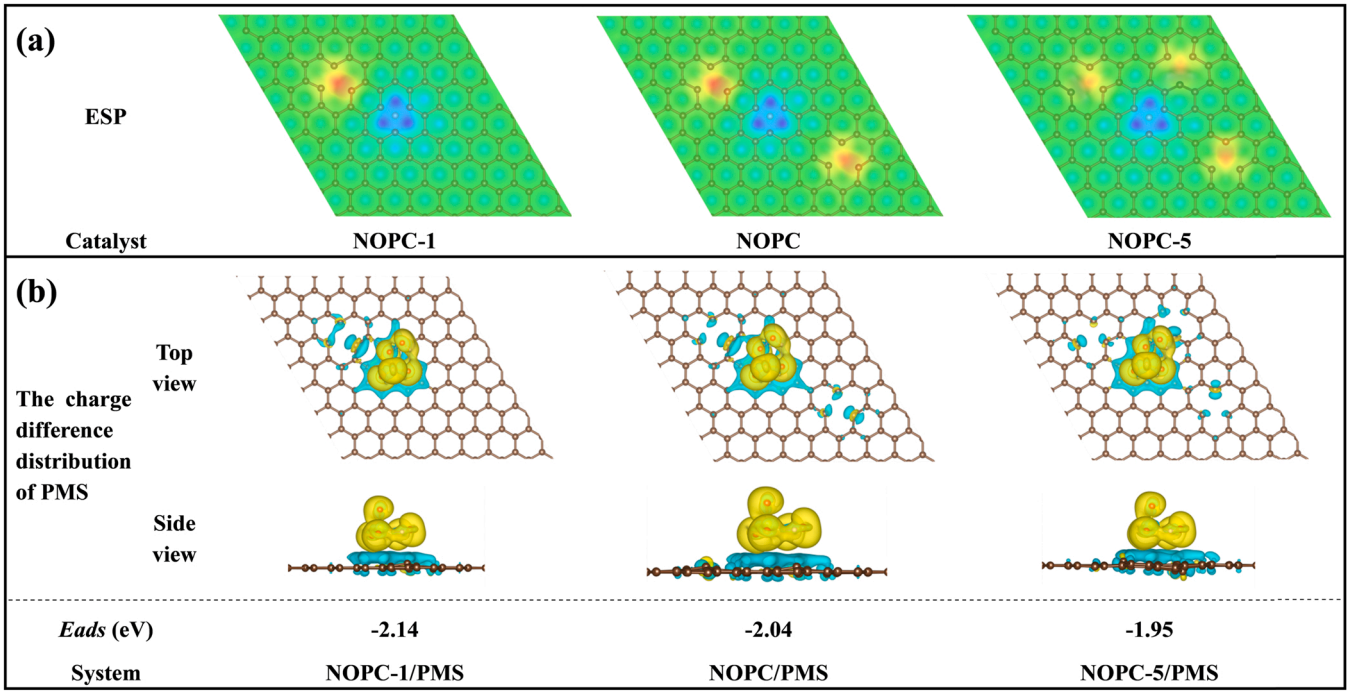

Fig. 8. ESP distribution (isosurface contour is 0.05 e/bohr^3) of NOPC-1, NOPC, NOPC-5 (a), the charge difference distribution of PMS and *Eads* in PMS/ NOPC-1, PMS/NOPC, PMS/ NOPC-5 systems (b).

amounts and the electron conductivity of NOPC-x improved with the increase of x, confirming the positive correlation between the unpaired electrons and electron conductivity of NOPC-x. Simultaneously, Fig. S13 (a)-(b) clearly exhibited the positive correlations ($R^2 \geq 0.97$) between the unpaired electrons concentration and electron conductivity of NOPC-1, NOPC-2, NOPC and the k_{obs} of BPA degradation in NOPC-x/PMS (x = 1, 2, 3) system, respectively. Therefore, stronger electron transfer ability of NOPC-x, deriving from more unpaired electrons, would result in more efficient BPA degradation in PMS/NOPC-x (x = 1, 2, 3) system via electron transport pathway. Accordingly, NOPC-5 with maximum surfaced unpaired electrons should possess the strongest catalytic activity. However, the degradation efficiency of BPA in PMS/NOPC system rose firstly but then decreased with continuous increase of unpaired electrons on the surface of NOPC-x (Fig. 7(b)– 7(c)). PMS has two dissociation constants, with $pK_{a1} < 0.0$ and $pK_{a2} = 9.4$. The pH of the solution remained about 5.5, which was less than the pK_{a2}. Therefore, PMS existed in the solution with a negative charge (HSO_5^-). As revealed in Fig. 7(a), extra unpaired electrons were generated on the

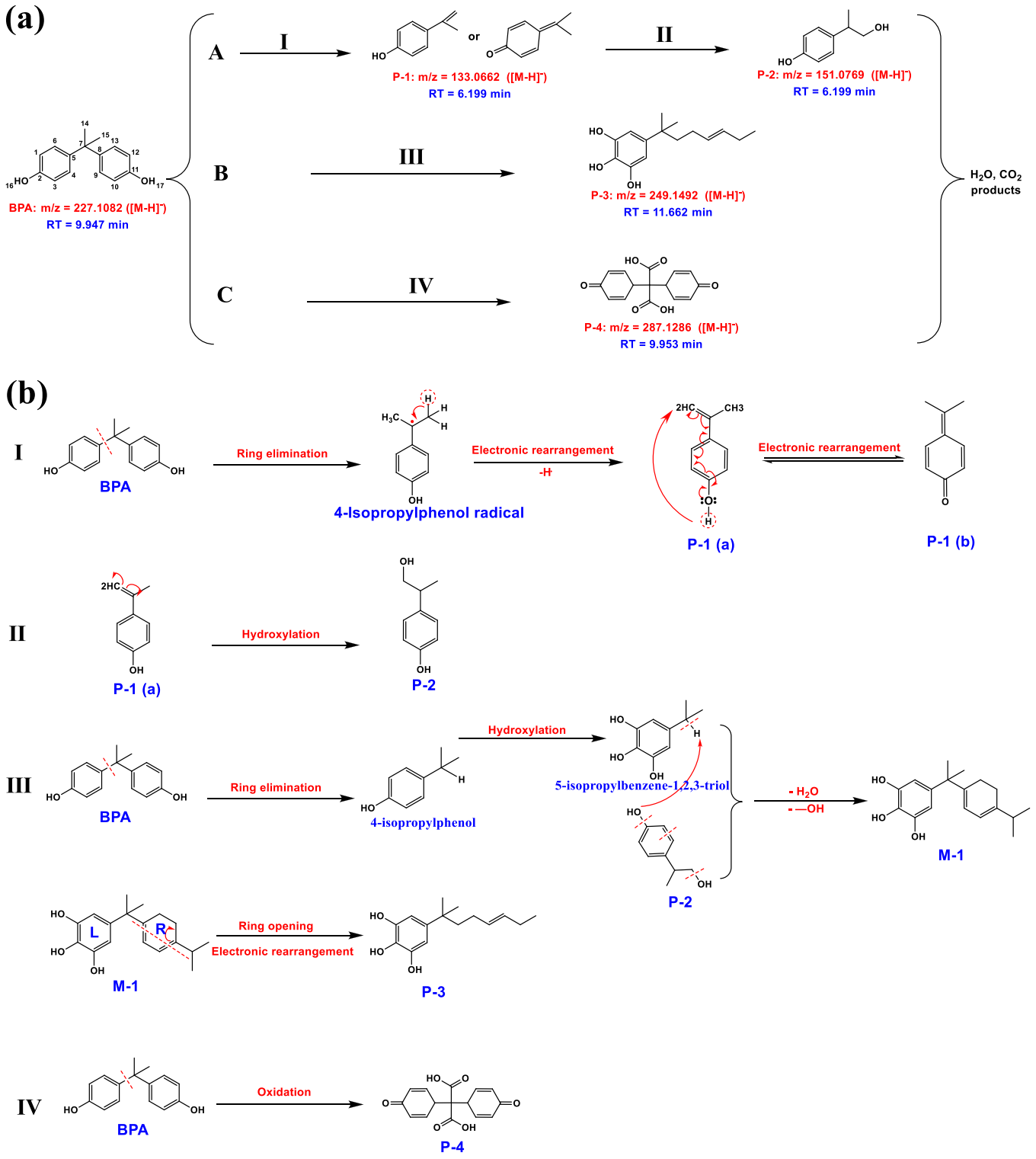

Scheme 2. Potential degradation pathways of BPA in NOPC/PMS system.

surface of C atoms due to the rupture of C-N bonds during the process of N atoms loss [32,33]. The excess electrons led NOPC negatively charged, since partial C atoms of NOPC had more electrons than protons [31,71,72]. The contact between HSO_5^- and NOPC could be hampered by the electrostatic repulsion [73]. Consequently, the adsorption capacity of NOPC-x for PMS linearly decreased with the enhancement of 'x', which might arise from the increased repulsion force between PMS (HSO_5^-) and NOPC-x along with the increase of surfaced unpaired electrons (Fig. 7 (d)) [74–76]. This phenomenon was also reflected by the adsorption energy between NOPC-x and PMS. Greater *Eads* means stronger adsorption between NOPC-x and PMS [77]. As shown in Fig. 8(b), the *Eads* decreased with the increase of 'x', resulting from the multiplying unpaired electrons. As such, it's speculated that the BPA removal efficiency might be a balance result of enhanced electron transfer, and increased repulsion force between PMS (HSO_5^-) and NOPC-x caused by the unpaired electrons.

3.5. Transformation products and degradation pathway of BPA

The degradation products of BPA in NOPC/PMS system were detected by UPLC-QTOF-MS/MS. Their structural formulas were derived from the *m/z* values of fragment ions and the related information was listed in Table S8 and Fig. S14-S18. Except for P-4, the error between the detected *m/z* and the exact *m/z* of the other products was less than or equal to 52 ppm. In addition, the calculated DBE is identical to the exact DBE of every product, indicating that all the speculated products have high reliability. Three pathways and four processes of BPA degradation were proposed as illustrated in Scheme 2 (a). C_5 and C_7 in BPA were electron-rich positions according to the frontier electron density on the carbon atoms of BPA [78]. Thus, BPA was split to produce 4-isopropylphenol radical with the C_5-C_7 bond rupture. Subsequently, P-1 (a) and/or P-1 (b) were produced via a series of electronic rearrangement on 4-Isopropylphenol radical (process I) [79]. In the process II, P-2 was produced by P-1 (a) with hydroxylation [80]. Similar to process I, 4-isopropylphenol was produced by the rupture of C_5-C_7 bond in BPA and transformed to 5-isopropylbenzene-1,2,3-triol via hydroxylation. Intermediate product (M-1, not detected in this work) was generated by the combination of 5-isopropylbenzene-1,2,3-triol and P-2 with the removal of one molecule H_2O and hydroxyl. P-3 was produced by the opening of right ring in M-1 followed electronic rearrangement [79]. The two methyl groups in BPA were oxidized to carboxyl groups to produce P-4 [81]. Finally, P-2, P-3 and P-4 were further degraded into H_2O, CO_2 with a result of obvious TOC removal, and other products.

Particularly, the intermediates could reflect the pollutants degradation mechanism. P-1, P-2 and P-4 of BPA were usually generated by direct electron transfer pathway [81]. Therefore, the existence of the typical intermediate products further proved that BPA was mainly degraded via electron transfer path in PMS/NOPC system.

4. Conclusions

In this study, a green carbon-catalyst (NOPC) for effective PMS activation and BPA oxidation was synthesized by co-pyrolysis of urea and mannitol. The excellent catalytic performance of NOPC was a result of the electron transfer capacity of graphitic N. PMS/NOPC system had excellent stability and showed high resistance to the presence of background substances. The radical scavenging experiments and EPR analysis unveiled that the BPA degradation by PMS/NOPC system neither depended on free radicals (HO•, $SO_4^{\bullet -}$, $O_2^{\bullet -}$) nor $^1O_2$. NOPC has a larger SA_{BET}, a higher content of graphite N, and a smaller electrical resistance, making NOPC favor electron transport during the BPA degradation process. The premixing experiments and electrochemical cell experiments confirmed that BPA could directly transfer electrons to PMS through NOPC. More importantly, this article explored the relationship between BPA removal and the surfaced unpaired electrons, whose amounts would be enhanced with the increase of modifier dosage. It was found that excessive unpaired electrons on NOPC surface was unfavorable to the degradation of pollutants, since superfluous unpaired electrons will hinder the contact between NOPC and PMS and further block the electron transfer. Therefore, in order to obtain satisfactory BPA degradation, controlling the number of unpaired electrons on NOPC surface in an appropriate range is necessary.

CRediT authorship contribution statement

Yong-Li He: Investigation, Methodology, Software, Data curation, Writing – original draft. **Chuan-Shu He:** Methodology, Data curation, Writing – review & editing. **Lei-Duo Lai:** Validation. **Peng Zhou:** Investigation. **Heng Zhang:** Methodology. **Ling-Li Li:** Data curation. **Zhao-Kun Xiong:** Software. **Yang Mu:** Writing – review & editing. **Zhi-Cheng Pan:** Methodology. **Gang Yao:** Supervision. **Bo Lai:** Supervision, Writing – review & editing, Funding acquisition.

Declaration of Competing Interest

The authors declare that they have no known competing financial interests or personal relationships that could have appeared to influence the work reported in this paper.

Acknowledgements

The authors thank the National Natural Science Foundation of China (52070133, 52170088, and 51808468) for financial supporting.

Appendix A. Supporting information

Supplementary data associated with this article can be found in the online version at doi:10.1016/j.apcatb.2022.121390.

References

[1] T. Geens, L. Goeyens, A. Covaci, Are potential sources for human exposure to bisphenol-A overlooked? Int. J. Hyg. Environ. Health 214 (2011) 339–347.
[2] V. Colborn, S. Saal, Developmental effects of endocrine-disrupting chemicals in wildlife and humans, Environ. Health Perspect. (1993).
[3] Y. Xu, A. Jia, H. Zhang, The mechanism of degradation of bisphenol A using the magnetically separable $CuFe_2O_4$/peroxymonosulfate heterogeneous oxidation process, J. Hazard. Mater. 309 (2016) 87–96.
[4] H. Zhang, Z. Xiong, F. Ji, B. Lai, P. Yang, Pretreatment of shale gas drilling flowback fluid (SGDF) by the microscale Fe^0/persulfate/O_3 process (mFe^0/PS/O_3), Chemosphere 176 (2017) 192–201.
[5] S. Wu, L. Shen, Y. Lin, K. Yin, C. Yang, Sulfite-based advanced oxidation and reduction processes for water treatment, Chem. Eng. J. 414 (2021).
[6] Y. Yuan, B. Lai, P. Yang, Y. Zhou, Treatment of ammunition wastewater by the combined Fe^0/air and Fenton process (1 st Fe^0/air-Fenton-2 nd Fe^0/air), J. Taiwan Inst. Chem. Eng. 65 (2016) 286–294.
[7] Y. He, J. Zhang, H. Zhou, G. Yao, B. Lai, Synergistic multiple active species for the degradation of sulfamethoxazole by peroxymonosulfate in the presence of CuO@FeO_x@Fe^0, Chem. Eng. J. 380 (2020), 122568.
[8] H. Zhou, L. Lai, Y. Wan, Y. He, G. Yao, B. Lai, Molybdenum disulfide (MoS_2): a versatile activator of both peroxymonosulfate and persulfate for the degradation of carbamazepine, Chem. Eng. J. 384 (2020).
[9] B. Huang, Z. Xiong, P. Zhou, H. Zhang, Z. Pan, G. Yao, B. Lai, Ultrafast degradation of contaminants in a trace cobalt(II) activated peroxymonosulfate process triggered through borate: Indispensable role of intermediate complex, J. Hazard. Mater. 424 (2022), 127641.
[10] S. Nimai, H. Zhang, Z. Wu, N. Li, B. Lai, Efficient degradation of sulfamethoxazole by acetylene black activated peroxydisulfate, Chin. Chem. Lett. 31 (2020) 2657–2660.
[11] H. Zhang, Q. Ji, L. Lai, G. Yao, B. Lai, Degradation of p-nitrophenol (PNP) in aqueous solution by mFe/Cu-air-PS system, Chin. Chem. Lett. (2019).
[12] S. Yanan, X. Xing, Q. Yue, B. Gao, Y. Li, Nitrogen-doped carbon nanotubes encapsulating Fe/Zn nanoparticles as a persulfate activator for sulfamethoxazole degradation: role of encapsulated bimetallic nanoparticles and nonradical reaction, Environ. Sci. Nano. 7 (2020) 1444–1453.
[13] J. Wang, S. Wang, Activation of persulfate (PS) and peroxymonosulfate (PMS) and application for the degradation of emerging contaminants, Chem. Eng. J. 334 (2018) 1502–1517.
[14] J. Sharma, I.M. Mishra, D.D. Dionysiou, V. Kumar, Oxidative removal of Bisphenol A by UV-C/peroxymonosulfate (PMS): kinetics, influence of co-existing chemicals and degradation pathway, Chem. Eng. J. 276 (2015) 193–204.

[15] Y.F. Huang, Y.H. Huang, Behavioral evidence of the dominant radicals and intermediates involved in bisphenol A degradation using an efficient Co^{2+}/PMS oxidation process, J. Hazard. Mater. 167 (2009) 418–426.

[16] J. Lee, U. von Gunten, J.-H. Kim, Persulfate-based advanced oxidation: critical assessment of opportunities and roadblocks, Environ. Sci. Technol. 54 (2020) 3064–3081.

[17] L. Li, L. Yang, R. Zou, J. Lan, J. Shang, B. Dou, H. Liu, S. Lin, Facile and scalable preparation of ZIF-67 decorated cotton fibers as recoverable and efficient adsorbents for removal of malachite green, J. Leather Sci. Eng. 3 (2021).

[18] P. Hu, H. Su, Z. Chen, C. Yu, Q. Li, B. Zhou, P.J.J. Alvarez, M. Long, Selective degradation of organic pollutants using an efficient metal-free catalyst derived from carbonized polypyrrole via peroxymonosulfate activation, Environ. Sci. Technol. 51 (2017) 11288–11296.

[19] X. Wang, K. Maeda, A. Thomas, K. Takanabe, G. Xin, J.M. Carlsson, K. Domen, M. Antonietti, A metal-free polymeric photocatalyst for hydrogen production from water under visible light, Nat. Mater. 8 (2009) 76–80.

[20] J. Li, Y. Zhang, X. Zhang, J. Han, Y. Wang, L. Gu, Z. Zhang, X. Wang, J. Jian, P. Xu, B. Song, Direct transformation from graphitic C_3N_4 to nitrogen-doped graphene: an efficient metal-free electrocatalyst for oxygen reduction reaction, ACS Appl. Mater. Interfaces 7 (2015) 19626–19634.

[21] J. Li, D. Wu, J. Iocozzia, H. Du, X. Liu, Y. Yuan, W. Zhou, Z. Li, Z. Xue, Z. Lin, Achieving efficient incorporation of pi-electrons into graphitic carbon nitride for markedly improved hydrogen generation, Angew. Chem. Int. Ed. Engl. 58 (2019) 1985–1989.

[22] W. Ma, N. Wang, Y. Fan, T. Tong, X. Han, Y. Du, Non-radical-dominated catalytic degradation of bisphenol A by ZIF-67 derived nitrogen-doped carbon nanotubes frameworks in the presence of peroxymonosulfate, Chem. Eng. J. 336 (2018) 721–731.

[23] Y. Gao, Y. Zhu, L. Lyu, Q. Zeng, X. Xing, C. Hu, Electronic structure modulation of graphitic carbon nitride by oxygen doping for enhanced catalytic degradation of organic pollutants through peroxymonosulfate activation, Environ. Sci. Technol. 52 (2018) 14371–14380.

[24] H. Wang, B. Wang, Y. Bian, L. Dai, Enhancing photocatalytic activity of graphitic carbon nitride by codoping with P and C for efficient hydrogen generation, ACS Appl. Mater. Interfaces 9 (2017) 21730–21737.

[25] Y. Gao, T. Li, Y. Zhu, Z. Chen, J. Liang, Q. Zeng, L. Lyu, C. Hu, Highly nitrogen-doped porous carbon transformed from graphitic carbon nitride for efficient metal-free catalysis, J. Hazard. Mater. 393 (2020), 121280.

[26] P. Qiu, C. Xu, H. Chen, F. Jiang, X. Wang, R. Lu, X. Zhang, One step synthesis of oxygen doped porous graphitic carbon nitride with remarkable improvement of photo-oxidation activity: Role of oxygen on visible light photocatalytic activity, Appl. Catal. B 206 (2017) 319–327.

[27] Y. Zhu, Z. Chen, Y. Gao, C. Hu, General synthesis of carbon and oxygen dual-doped graphitic carbon nitride via copolymerization for non-photochemical oxidation of organic pollutant, J. Hazard. Mater. 394 (2020), 122578.

[28] L. Wang, X. Lan, W. Peng, Z. Wang, Uncertainty and misinterpretation over identification, quantification and transformation of reactive species generated in catalytic oxidation processes: A review, J. Hazard. Mater. (2020), 124436.

[29] H. Lee, H.I. Kim, S. Weon, W. Choi, Y.S. Hwang, J. Seo, C. Lee, J.H. Kim, Activation of persulfates by graphitized nanodiamonds for removal of organic compounds, Environ. Sci. Technol. 50 (2016) 10134–10142.

[30] Q. Yang, Y. Chen, X. Duan, S. Zhou, Y. Niu, H. Sun, L. Zhi, S. Wang, Unzipping carbon nanotubes to nanoribbons for revealing the mechanism of nonradical oxidation by carbocatalysis, Appl. Catal. B 276 (2020), 119146.

[31] J. Xue, M. Fujitsuka, T. Majima, The role of nitrogen defects in graphitic carbon nitride for visible-light-driven hydrogen evolution, Phys. Chem. Chem. Phys. 21 (2019) 2318–2324.

[32] J. Jiang, X. Wang, Y. Liu, Y. Ma, T. Li, Y. Lin, T. Xie, S. Dong, Photo-Fenton degradation of emerging pollutants over Fe-POM nanoparticle/porous and ultrathin g-C_3N_4 nanosheet with rich nitrogen defect: Degradation mechanism, pathways, and products toxicity assessment, Appl. Catal. B 278 (2020), 119349.

[33] S. Zhu, X. Huang, F. Ma, L. Wang, X. Duan, S. Wang, Catalytic removal of aqueous contaminants on N-doped graphitic biochars: inherent roles of adsorption and nonradical mechanisms, Environ. Sci. Technol. 52 (2018) 8649–8658.

[34] J. Zhang, M. Zhang, G. Zhang, X. Wang, Synthesis of carbon nitride semiconductors in sulfur flux for water photoredox catalysis, ACS Catal. 2 (2012) 940–948.

[35] Q. Liang, Z. Li, Z.-H. Huang, F. Kang, Q.-H. Yang, Holey graphitic carbon nitride nanosheets with carbon vacancies for highly improved photocatalytic hydrogen production, Adv. Funct. Mater. 25 (2015) 6885–6892.

[36] H.-Q. Zhao, Q. Liu, Y.-X. Wang, Z.-Y. Han, Z.-G. Chen, Y. Mu, Biochar enhanced biological nitrobenzene reduction with a mixed culture in anaerobic systems: Short-term and long-term assessments, Chem. Eng. J. 351 (2018) 912–921.

[37] J. Peng, P. Zhou, H. Zhou, W. Liu, H. Zhang, C. Zhou, L. Lai, Z. Ao, S. Su, B. Lai, Insights into the electron-transfer mechanism of permanganate activation by graphite for enhanced oxidation of sulfamethoxazole, Environ. Sci. Technol. (2021).

[38] H. Zhou, J. Peng, J. Li, J. You, L. Lai, R. Liu, Z. Ao, G. Yao, B. Lai, Metal-free black-red phosphorus as an efficient heterogeneous reductant to boost Fe(3+)/Fe(2+) cycle for peroxymonosulfate activation, Water Res. 188 (2021), 116529.

[39] S. Zhang, Y. Liu, P. Gu, R. Ma, T. Wen, G. Zhao, L. Li, Y. Ai, C. Hu, X. Wang, Enhanced photodegradation of toxic organic pollutants using dual-oxygen-doped porous g-C_3N_4: Mechanism exploration from both experimental and DFT studies, Appl. Catal. B 248 (2019) 1–10.

[40] Q. Liu, J. Shen, X. Yu, X. Yang, W. Liu, J. Yang, H. Tang, H. Xu, H. Li, Y. Li, J. Xu, Unveiling the origin of boosted photocatalytic hydrogen evolution in simultaneously (S, P, O)-Codoped and exfoliated ultrathin g-C_3N_4 nanosheets, Appl. Catal. B 248 (2019) 84–94.

[41] J. Chen, Z. Mao, L. Zhang, D. Wang, R. Xu, L. Bie, B.D. Fahlman, Nitrogen-deficient graphitic carbon nitride with enhanced performance for lithium ion battery anodes, ACS Nano 11 (2017) 12650–12657.

[42] W. Ma, Y. Du, N. Wang, P. Miao, ZIF-8 derived nitrogen-doped porous carbon as metal-free catalyst of peroxymonosulfate activation, Environ. Sci. Pollut. Res. Int. 24 (2017) 16276–16288.

[43] X. Duan, H. Sun, Y. Wang, J. Kang, S. Wang, N-doping-induced nonradical reaction on single-walled carbon nanotubes for catalytic phenol oxidation, ACS Catal. 5 (2014) 553–559.

[44] G. Wang, S. Chen, X. Quan, H. Yu, Y. Zhang, Enhanced activation of peroxymonosulfate by nitrogen doped porous carbon for effective removal of organic pollutants, Carbon 115 (2017) 730–739.

[45] K. Schwinghammer, M.B. Mesch, V. Duppel, C. Ziegler, J. Senker, B.V. Lotsch, Crystalline carbon nitride nanosheets for improved visible-light hydrogen evolution, J. Am. Chem. Soc. 136 (2014) 1730–1733.

[46] Y. Gao, Z. Chen, Y. Zhu, T. Li, C. Hu, New Insights into the generation of singlet oxygen in the metal-free peroxymonosulfate activation process: important role of electron-deficient carbon atoms, Environ. Sci. Technol. 54 (2020) 1232–1241.

[47] X. Duan, H. Sun, S. Wang, Metal-free carbocatalysis in advanced oxidation reactions, Acc. Chem. Res. 51 (2018) 678–687.

[48] M. Xu, H. Zhou, Z. Wu, N. Li, Z. Xiong, G. Yao, B. Lai, Efficient degradation of sulfamethoxazole by $NiCo_2O_4$ modified expanded graphite activated peroxymonosulfate: Characterization, mechanism and degradation intermediates, J. Hazard. Mater. 399 (2020), 123103.

[49] Y. Li, J. Li, Y. Pan, Z. Xiong, G. Yao, R. Xie, B. Lai, Peroxymonosulfate activation on $FeCo_2S_4$ modified g-C_3N_4 ($FeCo_2S_4$-CN): Mechanism of singlet oxygen evolution for nonradical efficient degradation of sulfamethoxazole, Chem. Eng. J. 384 (2020), 123361.

[50] G. Zhang, M. Zhang, X. Ye, X. Qiu, S. Lin, X. Wang, Iodine modified carbon nitride semiconductors as visible light photocatalysts for hydrogen evolution, Adv. Mater. 26 (2014) 805–809.

[51] L. Lai, H. Zhou, B. Lai, Heterogeneous degradation of bisphenol A by peroxymonosulfate activated with vanadium-titanium magnetite: Performance, transformation pathways and mechanism, Chem. Eng. J. 349 (2018) 633–645.

[52] Y. Li, X. Zhao, Y. Yan, J. Yan, Y. Pan, Y. Zhang, B. Lai, Enhanced sulfamethoxazole degradation by peroxymonosulfate activation with sulfide-modified microscale zero-valent iron (S-mFe^0): Performance, mechanisms, and the role of sulfur species, Chem. Eng. J. 376 (2019), 121302.

[53] L. Lai, H. Zhou, H. Zhang, Z. Ao, Z. Pan, Q. Chen, Z. Xiong, G. Yao, B. Lai, Activation of peroxydisulfate by natural titanomagnetite for atrazine removal via free radicals and high-valent iron-oxo species, Chem. Eng. J. 387 (2020), 124165.

[54] Z. Wang, J. Wang, B. Xiong, F. Bai, S. Wang, Y. Wan, L. Zhang, P. Xie, M. R. Wiesner, Application of cobalt/peracetic acid to degrade sulfamethoxazole at neutral condition: efficiency and mechanisms, Environ. Sci. Technol. 54 (2020) 464–475.

[55] S.H. Ho, Y.D. Chen, R. Li, C. Zhang, Y. Ge, G. Cao, M. Ma, X. Duan, S. Wang, N. Q. Ren, N-doped graphitic biochars from C-phycocyanin extracted Spirulina residue for catalytic persulfate activation toward nonradical disinfection and organic oxidation, Water Res. 159 (2019) 77–86.

[56] A. Juan, L. Konrad S., Degradation kinetics of atrazine and its degradation products with ozone and OH radicals: a predictive tool for drinking water treatment, Environ. Sci. Technol. 34 (2000) 591–597.

[57] W.D. Oh, Z. Dong, G. Ronn, T.T. Lim, Surface-active bismuth ferrite as superior peroxymonosulfate activator for aqueous sulfamethoxazole removal: Performance, mechanism and quantification of sulfate radical, J. Hazard. Mater. 325 (2017) 71–81.

[58] S. Enami, Y. Sakamoto, A.J. Colussi, Fenton chemistry at aqueous interfaces, Proc. Natl. Acad. Sci. U. S. A. 111 (2014) 623–628.

[59] G. Fang, T. Zhang, H. Cui, D.D. Dionysiou, C. Liu, J. Gao, Y. Wang, D. Zhou, Synergy between Iron and selenide on $FeSe_2$(111) surface driving peroxymonosulfate activation for efficient degradation of pollutants, Environ. Sci. Technol. 54 (2020) 15489–15498.

[60] D. Dai, Z. Yang, Y. Yao, L. Chen, G. Jia, L. Luo, Highly efficient removal of organic contaminants based on peroxymonosulfate activation by iron phthalocyanine: mechanism and the bicarbonate ion enhancement effect, Catal. Sci. Technol. 7 (2017) 934–942.

[61] W. Su, J. Chen, L. Wu, X. Wang, X. Wang, X. Fu, Visible light photocatalysis on praseodymium(III)-nitrate-modified TiO_2 prepared by an ultrasound method, Appl. Catal. B 77 (2008) 264–271.

[62] C. Qi, X. Liu, J. Ma, C. Lin, X. Li, H. Zhang, Activation of peroxymonosulfate by base: Implications for the degradation of organic pollutants, Chemosphere 151 (2016) 280–288.

[63] F. Yang, Y. Huang, C. Fang, Y. Xue, L. Ai, J. Liu, Z. Wang, Peroxymonosulfate/base process in saline wastewater treatment: The fight between alkalinity and chloride ions, Chemosphere 199 (2018) 84–88.

[64] E.T. Yun, J.H. Lee, J. Kim, H.D. Park, J. Lee, Identifying the nonradical mechanism in the peroxymonosulfate activation process: singlet oxygenation versus mediated electron transfer, Environ. Sci. Technol. 52 (2018) 7032–7042.

[65] Y. Yang, G. Banerjee, G.W. Brudvig, J.H. Kim, J.J. Pignatello, Oxidation of organic compounds in water by unactivated peroxymonosulfate, Environ. Sci. Technol. 52 (2018) 5911–5919.

[66] Y. Zhou, J. Jiang, Y. Gao, J. Ma, S.Y. Pang, J. Li, X.T. Lu, L.P. Yuan, Activation of peroxymonosulfate by benzoquinone: a novel nonradical oxidation process, Environ. Sci. Technol. 49 (2015) 12941–12950.

[67] N. Vol, A Europium(lll) complex as an efficient singlet oxygen luminescence probe, J. Am. Chem. Soc. (2006) 13442–13450.
[68] R. Luo, M. Li, C. Wang, M. Zhang, M.A. Nasir Khan, X. Sun, J. Shen, W. Han, L. Wang, J. Li, Singlet oxygen-dominated non-radical oxidation process for efficient degradation of bisphenol A under high salinity condition, Water Res. 148 (2019) 416–424.
[69] H. Cai, J. Zou, J. Lin, J. Li, Y. Huang, S. Zhang, B. Yuan, J. Ma, Sodium hydroxide-enhanced acetaminophen elimination in heat/peroxymonosulfate system: Production of singlet oxygen and hydroxyl radical, Chem. Eng. J. 429 (2022).
[70] H. Lee, H.-J. Lee, J. Jeong, J. Lee, N.-B. Park, C. Lee, Activation of persulfates by carbon nanotubes: oxidation of organic compounds by nonradical mechanism, Chem. Eng. J. 266 (2015) 28–33.
[71] R. Glaser, G.S.-C. Choy, G.S. Chen, H. Grützmacher, Inductive and conjugative S→C Polarizations in "Trithiocarbenium Ions" $[C(SH)_3]^+$ and $[C(SH)_3]^{\bullet,2+}$. potential energy surface analysis, electronic structure motif, and spin density distribution, J. Am. Chem. Soc. 118 (1996) 11617–11628.
[72] H.A. Harris, D.R. Kanis, L.F. Dahl, A comparative theoretical analysis of the physicochemically dissimilar tetrathiolate- and oxalate-bridged dititanium series, $[(Cp_2Ti)_2(\mu\text{-}C_2X_4)]n$ (where X = S, n = 0, 1-, 2-; X = O, n = 0, 2+): an explanation of electron delocalization from the metal centers upon replacement of the oxalate ligand with the tetrathiooxalate ligand, J. Am. Chem. Soc. 113 (1991) 8602–8611.
[73] T. Katagiri, S. Yamaji, M. Handa, M. Irie, K. Uneyama, Diastereoselectivity controlled by electrostatic repulsion between the negative charge on a trifluoromethyl group and that on aromatic rings, Chem. Commun. (Camb.) (2001) 2054–2055.
[74] Q. Qin, X. Gao, X. Wu, Y. Liu, NaBH4-treated cobalt-doped g-C_3N_4 for enhanced activation of peroxymonosulfate, Mater. Lett. 256 (2019).
[75] W. Ren, L. Xiong, G. Nie, H. Zhang, X. Duan, S. Wang, Insights into the Electron-transfer regime of peroxydisulfate activation on carbon nanotubes: the role of oxygen functional groups, Environ. Sci. Technol. 54 (2020) 1267–1275.
[76] W. Ren, L. Xiong, X. Yuan, Z. Yu, H. Zhang, X. Duan, S. Wang, Activation of peroxydisulfate on carbon nanotubes: electron-transfer mechanism, Environ. Sci. Technol. 53 (2019) 14595–14603.
[77] J. You, W. Sun, S. Su, Z. Ao, C. Liu, G. Yao, B. Lai, Degradation of bisphenol A by peroxymonosulfate activated with oxygen vacancy modified nano-NiO-ZnO composite oxides: A typical surface-bound radical system, Chem. Eng. J. 400 (2020), 125915.
[78] N. Watanabe, S. Horikoshi, H. Kawabe, Y. Sugie, J. Zhao, H. Hidaka, Photodegradation mechanism for bisphenol A at the TiO_2/H_2O interfaces, Chemosphere 52 (2003) 851–859.
[79] W.H.M. Abdelraheem, M.K. Patil, M.N. Nadagouda, D.D. Dionysiou, Hydrothermal synthesis of photoactive nitrogen- and boron- codoped TiO_2 nanoparticles for the treatment of bisphenol A in wastewater: Synthesis, photocatalytic activity, degradation byproducts and reaction pathways, Appl. Catal. B 241 (2019) 598–611.
[80] J. Gao, X. Duan, K. O'Shea, D.D. Dionysiou, Degradation and transformation of bisphenol A in UV/Sodium percarbonate: dual role of carbonate radical anion, Water Res. 171 (2020), 115394.
[81] X.Y. Pei, H.Y. Ren, G.S. Liu, G.L. Cao, G.J. Xie, D.F. Xing, N.Q. Ren, B.F. Liu, Non-radical mechanism and toxicity analysis of beta-cyclodextrin functionalized biochar catalyzing the degradation of bisphenol A and its analogs by peroxydisulfate, J. Hazard. Mater. 424 (2022), 127254.